

Electromagnetic Field Analysis of the Performance of Single-Phase Capacitor-Run Induction Motor Using Composite Rotor Conductor

Mohd Afaque Iqbal*, Gurmeet Singh**

*(Department of Electrical & Instrumentation, SLIET Longowal University, Punjab-148106)

** (Department of Electrical & Instrumentation, SLIET Longowal University, Punjab-148106)

ABSTRACT

Single-phase induction motor (SPIM) has very crucial role in industrial, domestic and commercial sectors. So, the efficient SPIM is a major requirement of today's market. For efficient motors, many research methodologies and suggestions have been given by researchers in past. Various parameters like as stator/rotor slot variation, size and shape of stator/rotor slots, stator/rotor winding configuration, choice of core material etc. have significant impact on machine design. Rotor slot geometry influences the distribution of the magnetic field to a degree. Even a little difference of the magnetic field distribution can make big difference on the performance of the induction motor. The rotor slot geometry influences the skin effect and slot leakage flux in order to increase the torque and efficiency. In this paper, three types of rotor slot configurations are designed and simulated with different rotor slot configuration and rotor bars composition by changing the rotor slot configuration of base model. Aluminum and Copper are used simultaneously as rotor winding material. The rotor bar is a composite conductor which carries Aluminum as well as Copper sub-conductors running parallel in the same slot. Overall cross section area of rotor bar in each model kept same and work is carried out with difference proportion of Aluminum and Copper sub conductors. All models are investigated and simulated in FEMM and finally the simulated results are compared for optimal solution.

Keywords - Single-Phase induction motor, rotor winding, rotor geometry, composite conductor, FEMM.

I. Introduction

Single Phase Induction Motor is a requisite motor out of electric motors. The features of SPIM are indistinguishable to three-phase induction motor except that SPIM has no inherent starting torque and some superior arrangements have to be made for making it self starting. These motors are generally used in industrial, commercial as well as in domestic zones because of their size, cost, weight, consistency and ease of maintenance [1].

Single phase induction motor requires just one power phase for its operation. These are commonly used in low power rating applications. Due to inexpensiveness and reliability in size, SPIMs are extensively used in industry especially in fractional kilowatt range motors. These motors can be directly connected to an AC power source. SPIMs are broadly classified into Split-phase, Capacitor run, and Capacitor start/run induction motor. The problem of poor starting torque in split-phase motors has solved by using a start capacitor in series with the auxiliary winding. Start capacitor may be disconnected after starting. Out of all types of SPIMs, the Capacitor-run induction motor is the most prevalent motor and broadly used because of their good starting and running physiognomies. Capacitor is permanently connected in series with auxiliary winding. An

adequately high starting torque produces by using capacitor which generates a leading phase current in the starting winding and motor operates as a balanced two phase machine [2]. Capacitor-run induction motor has poor starting torque performance because it's rotating magnetic field is oval shaped in air-gap [3].

Recently, many studies and researches have been done to improve the performance of SPIM by optimizing the design parameters. Some research has focused on core material of stator/rotor, some on slot variation & slot shape of stator/rotor, some on stator winding & capacitor value but rotor winding has paid least emphasis. Magnitude flux distribution in the induction motor is a major factor affecting the performance of the machine. The flux linkage with the rotor as well as rotor bar has a large influence on the nature of the torque developed by the machine. More circular field distribution leads to the better performance. Most of the work in past was carried out for electromagnetic field computation of main field/stator field but the distribution of magnetic field in the air-gap and approach to its uniformity has also paid least emphasis. A lot of simulation work in Matlab and other sophisticated software is done to adjust the design parameter for optimal performance but least emphasis about rotor slot. Currently, the

optimization work focus on the improvement of starting performance. This paper presents the effect of rotor winding configuration and distribution of flux on the performance of machine using Finite Element Method of Magnetic (FEMM). Three types of rotor slot configurations are investigated. The results obtained are compared with each other for optimal solution.

II. Finite Element Method of Magnetics

FEMM is used for solving low frequency electromagnetic problems on two-dimensional planar and axisymmetric domains. By the use of FEMM, magnetic field distribution can be easily computed. The major benefit of FEMM is that it is free of cost and easily available on internet. Easiness in control is additional advantage. Tactlessly, the FEMM cannot work with multifaceted three-dimensional models. Geometrical models can be formed unswervingly in FEMM, but drawing is uncomfortable. Auto-CAD designing is another possibility to draw a geometrical model [4]. Designed models in Auto-CAD must be saved in .dxf format because FEMM allows only .dxf files. So after designed, these models imported in FEMM.

III. Motor Geometry

In this work, squirrel cage motor with two-pole, 24 stator and 18 rotor slots is used as base model. The overview of reference model of the machine is shown in fig. 1 [3]. However, the rotor slot winding configuration of designed motor has been changed in the present work and all four models are simulated.

The specification of machine used under test is given in table 1 and the design parameters are shown in table 2 [3].

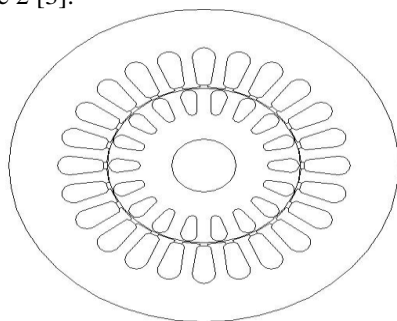


Fig. 1: overview of base model

TABLE 1: Specification of machine under test

| Parameters | Specification |
|-----------------------|---------------|
| Rated Power Output | 250 W |
| Rated Voltage | 220 V |
| Number of Poles | 2 |
| Rotor Position | Inner |
| Type of load | Constant |
| Operating Temperature | 75°C |
| Capacitor | 8 μF |

TABLE 2: Design parameters of Stator/Rotor

| Parameters | Specification |
|----------------------------|-----------------------|
| Number of stator slots | 24 |
| Outer diameter of stator | 120 mm |
| Inner diameter of stator | 60 mm |
| Length of stator core | 45 mm |
| Type of stator/rotor steel | Silicon core iron |
| Air gap | 0.3 mm |
| Outer diameter of rotor | 59.4 mm |
| Inner diameter of rotor | 20 mm |
| Length of rotor | 45 mm |
| Area of rotor slot | 38.80 mm ² |
| Number of rotor slots | 18 |
| Rotor speed | 720 rpm |

The research work is carried out to examine the influence of the rotor winding on the performance of the machine. In the simulation work, two materials aluminum and copper are concurrently used in the rotor winding to analyze the effects on the performance of the machine.

IV. Simulation work

In simulation work, four different configurations of the squirrel cage single phase capacitor run induction motor are examined by changing the rotor winding configurations. The other specifications like number of stator and rotor slots, length, diameter of stator and rotor core, stator and rotor slot area, input current and core material etc. kept unchanged.

The simulation work is carried out in two parts;

- 1.1 Auto-CAD based work
- 1.2 FEMM based work

4.1 Auto-CAD based work

All models are designed in Auto-CAD (version 2006) software. All models are designed with the specified dimensions in Auto-CAD. The shape and the configurations of the models have been changed from one model to another. The area of rotor slot kept same in all models which is equal to the area of base model. Half symmetry of the models is designed for simplicity. After designing these models, the files are saved in .dxf format because FEMM software allows only .dxf format files.

4.1.1 Geometry of rotor slots

In the simulation work the parameters of rotor slots for all three configurations along with base model used are given in table 3 and the final geometry obtained in the simulation work shown in fig. 2.

TABLE 3: Rotor slot parameter

| Parameter | Base Model | Model-I | Model-II | Model-III |
|-----------|------------|---------|----------|-----------|
| Hs0 (mm) | 2 | 2 | 2 | 2 |
| Bs0 (mm) | 0.3 | 0.3 | 0.3 | 0.3 |
| Hs1 (mm) | 5.75 | 3.515 | 3.515 | 3.515 |
| Hs2 (mm) | 2.6 | - | 1.757 | 2.343 |
| Hs3 (mm) | 1.6 | - | - | 1.172 |

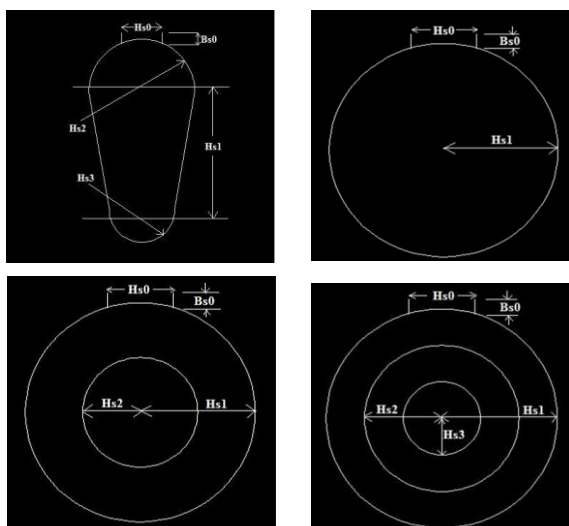


Fig. 2: rotor slots configuration

4.1.2 FEMM based work

All designed models are imported in FEMM. After importing the models, problem is defined and the boundary conditions are also set manually. Material is assigned to the model and boundary conditions are given to model. After this, mesh of the simulated model is created.

Aluminum and Copper are used simultaneously as rotor winding material. Rotor winding configuration of all models is shown in fig. 3.

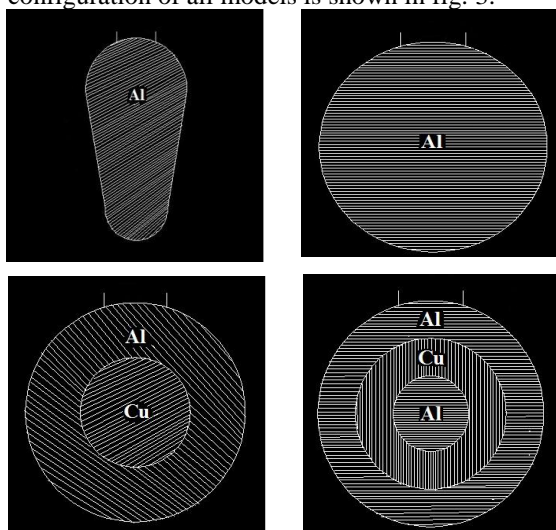


Fig. 3: rotor winding configuration

Now the machine is allowed to run at this stage. By the running of machine the results are evaluate and compared to each other for optimal solution. At last, the best optimal design is find out.

V. Results & Discussion

The results of simulation work obtained are recorded in table 4, for the comparison of all three models with base model. Wide variation in output parameters eventually reflects the influence of slot configuration on the performance of SPIM.

TABLE 4: Comparison of results

| Parameter | Base Model | Model-I | Model-II | Model-III |
|----------------------------------------|------------|-----------|-----------|-----------|
| Magnetic field energy (Joule) | 2.72e-09 | 1.49e-09 | 1.52e-009 | 1.52e-009 |
| Total losses (Watt) | 2.78e-06 | 2.74e-06 | 2.34e-06 | 2.24e-006 |
| Lorentz Torque (N*m) | 0.27e-12 | 9.33e-12 | 9.16e-12 | 9.30e-12 |
| Total loss density (W/m ³) | 0.178 | 0.174 | 0.149 | 0.142 |
| Voltage drop (Volt) | 0.0146 | 0.0263 | 0.0257 | 0.0255 |
| Real power (Watt) | 8.08e-06 | 5.77e-06 | 5.79e-06 | 5.79e-06 |
| Reactive power (VAr) | -2.78e-06 | -2.74e-06 | -2.34e-06 | -2.24e-06 |
| Apparent power (VA) | 8.55e-06 | 6.39e-06 | 6.25e-06 | 6.21e-06 |
| Power factor | 0.9456 | 0.9034 | 0.9270 | 0.9328 |
| Efficiency (%) | 79.81 | 80.12 | 82.98 | 83.75 |

5.1 Effects of Flux distribution and flux density

The flux distribution in each and every part of the machine is very important parameter for the performance of the machine. Rotor slot geometry influences the distribution of the magnetic field to a degree. The flux density plots of all simulated models are shown in fig. 4 (a), (b), (c), (d) with density scale.

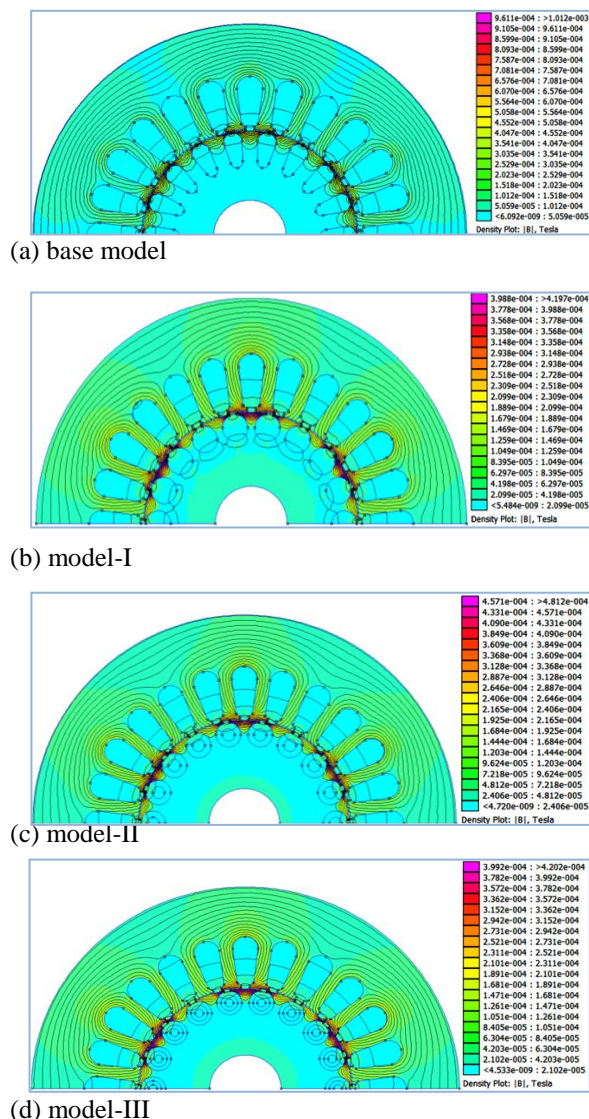


Fig. 4: flux density plot

The flux distribution of Base model shows that it has not sinusoidal waveform between stator and rotor i.e. in the air-gap. Formation of hot spot in the stator core beyond the slots results the local temperature rise and reducing the life of winding insulation. The total area in saturation for conduction path is more which leads in the eddy current and hysteresis losses. The leakage flux is also more in the conduction path of the machine. The highest density is recorded as 9.611e-004 from the density scale as shown in fig. 4(a). The density is more near about the slots but it decrease as far as from the slots. The flux density in rotor core is given below.

$$\text{Flux density in rotor core } B_{cr} = \frac{\phi_m}{(2 \times L_i \times d_{cr})}$$

Where d_{cr} = depth of rotor core

So, depth of rotor core is inversely proportional to flux density. It means that if the depth of rotor core is more, then the flux density will be less. So, flux

density is low around shaft and more in air-gap region. It can be seen from fig. 4.

The flux distribution in the Mode-I shows that it formed a sinusoidal form in the air-gap region as shown in fig. 4(b). With the sinusoidal form of the flux distribution the harmonics will be less that's why the total losses will be less as compared to base model. Flux density in the region of stator core at the back side of slots is small and the total area in saturation for conduction path is small which where reduce the eddy current as well as hysteresis losses and also the leakage flux in the machine. The highest density in the Model-I is recorded as 3.988e-004 which is lesser than that of base model. But in the air-gap region, the flux density is more comparatively to the base model. The flux density is 1.049e-004 near about the slot. So the flux density is more than that of in base model. So, Model-I has better results in comparison of base model which are reflected in table 4.

Flux distribution in Model-II has more effectively results compared to base model as well as Model-I. The flux distribution is more sinusoidal in this model as compared to base model and model-I. The area of conducting path is much smaller and the eddy current & hysteresis losses are much smaller. The region of conduction is more concentrated in this model as shown in fig. 4(c). The density scale shows the flux density in the machine. The highest flux density is recorded as 4.571e-004 in this model which is comparatively less than that of base model and slightly higher than that of model-I.

Model-III has better results among all the models. The flux distribution can be seen from the fig. 4(d). The flux is distributed in more sinusoidal form as compared to other models. The highest flux density has been recorded as 3.992e-004 which is less than all models except model-I. The area of conduction is more concentrated that's why the eddy current & hysteresis losses are less which is highlighted in table 4.

So, by the above discussion it has been concluded that Model-III is best optimal model because the losses are lesser compared to other models as reflected in table 4. The above discussion and the flux density plots of all models reflected the decrement in skin effect in the rotor bars by using the composite conductors in rotor bars.

5.2 Effects on Efficiency

The efficiency of the models is evaluated from the data presented in table 4. The efficiency is calculated with the help of following formula;

$$\eta = \frac{P_{out}}{P_{in}} \quad (1)$$

where P_{out} = Total losses + P_{in}

The evaluated efficiency for all models is shown in fig. 5 in bar graph. The calculated efficiency of base model recorded as 79.81 % whereas it is 80.12

% of Model-I which is slightly more than that of base model because in model-I the rotor slot is of circular shape by which the flux distribution is in sinusoidal form and the harmonics is less that's why the losses also less. The efficiency in Model-II is recorded as 82.98 % which is more than that of base model and model-I because aluminum & copper are simultaneously used as rotor winding material. The calculated efficiency of Model-III is 83.75 %. So, Model-III has more efficiency compared to all models. The efficiency is increased 3.94 % in Model-III as compared to that of base model. This incremental percentage in efficiency has imperative role in the performance of the SPIM.

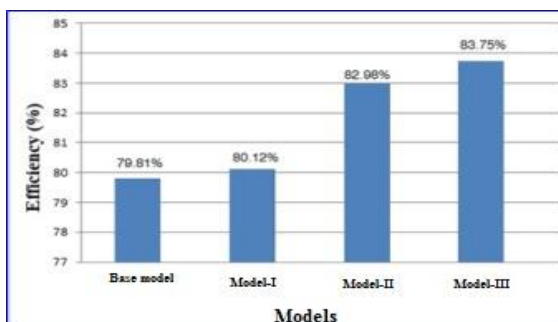


Fig. 5: Bar graph of efficiency

This improvement in the efficiency, because of better magnetic properties & higher operating flux density compared to other models. So the Model-III has better enhancement in efficiency and is the best optimized model compared to all other models.

5.3 Effects on Power factor

The Power factor is evaluated with the help of data presented in table 5. The bar graph of Power factor is shown in fig. 6. The calculated power factor for base model is 0.9456. Model-I has power factor of 0.9034 which is lower than that of base model but power factor for Model-II is 0.9270 which is more than that of Model-I but less than that of base model. While it is 0.9328 for Model-III which is more than that of Model-I and Model-II but slightly truncated as compared to that of base model. There is no more effect of Power factor on the performance of the machine as in Model-III.

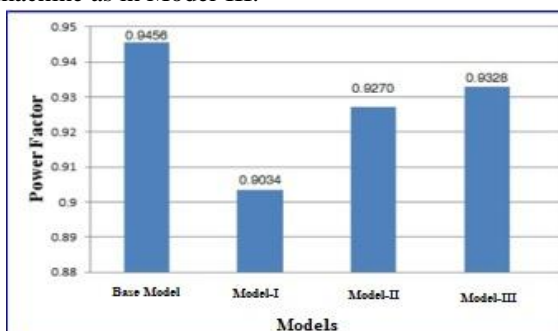


Fig. 6: Bar graph of power factor

Power factor has direct dependency on core material while this research work is based on rotor winding configuration. So, power factor has not significance here.

5.4 Effects on Lorentz torque

The Lorentz torque bar graph is shown in fig. 7. Torque is recorded as 0.27e-012 N*m in the base model while it is recorded 9.33e-012 N*m in Model-I which is higher than that of base model. Model-II has 9.16e-012 N*m and Model-III has 9.30e-012 N*m torque. Highest torque is recorded in case of Model-I. However torque of Model-II & Model-III is more as compared to base model.

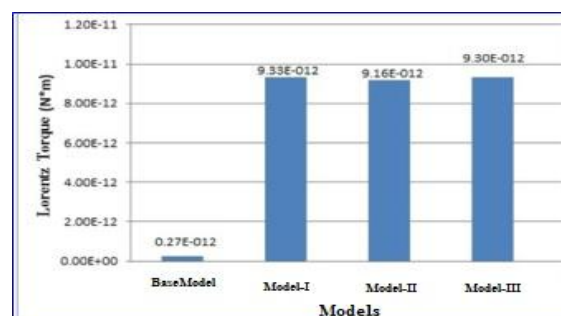


Fig. 7: Bar graph of Lorentz torque

5.5 Effects on Total losses

The bar graph of Total losses in all the models is shown in fig. 8. The total losses for the Base model are recorded as 2.781e-06 watt which is higher than that of all three models. Lowest losses are recorded as 2.238e-06 watt in Model-3. Model-I has losses of 2.739e-06 watt which are lesser than that of base model. Model-II has total losses of 2.334e-06 watt. So, Model-III has much lesser total losses as compared to the Base model. So in model-III total losses are lesser than other models and the performance of model-III increased compared to base model and all other simulated models.

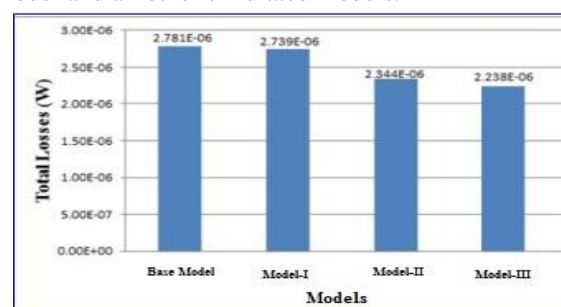


Fig. 8: Bar graph of total losses

5.5 Effects on Total loss density

The Total loss density is reflected in table 4 and the bar graph of total loss density of all models is shown in fig. 9. The Total loss density is 0.178 w/m³ for the Base model which is very high than that of all three models. Model-III has less total loss density compared to other models. Model-III has 0.142 w/m³

loss density. Model-I has 0.174 W/m^3 loss density, lower than that of base model. Total loss density of Model-II is 0.149 W/m^3 is also less than that of Model-I and base model.

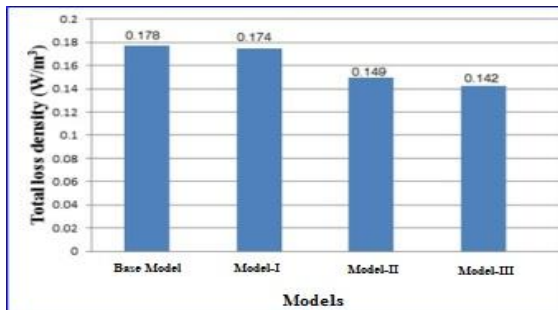


Fig. 9: Bar graph of total loss density

So, by the above discussion, Model-III is the best optimized model out of the three models investigated in the paper.

VI. Conclusion

Magnitude flux distribution in the induction motor is a major factor affecting the performance of the machine. The flux linkage with the rotor as well as rotor bar has a large influence on the nature of the torque developed by the machine. More circular field distribution leads to the better performance. Rotor geometry and rotor winding are the major components that play a vital role in optimization of performance of the machine. In this paper, four models of rotor has been designed and simulated with different rotor slot configuration and rotor bars composition. The rotor bar is a composite conductor which carries Aluminum as well as Copper sub-conductors running parallel in the same slot. Overall cross section area of rotor bar in each model kept same and work is carried out with difference proportion of Aluminum and Copper sub conductors. Model-III with 66.67 % aluminum and 33.33 % copper gives better results. With the increase in percentage of copper further provide better performance but at higher manufacturing cost. The efficiency in this model is 83.75 % as compared to 79.81 % of the base model. Model-III offered highest efficiency, highest torque and minimum losses and is the optimized model out of the three models simulated and base model.

References

[1] Sobhan Sobhani, Hamid Yaghoobi and Mehdi Samakoosh, *Optimize Efficiency and Torque in the Single-Phase Induction Motor by Adjusting the Design Parameters, Environment and Electrical Engineering international conference (EEEIC) 2013*, 237-241.

[2] C. Mademlis, I. Kioskeridis and T. Theodoulidis, *Optimization of Single-Phase Induction Motors- Part I: Maximum Energy Efficiency Control, IEEE Transactions on Energy Conversion*, Vol. 20, No. 1, March 2005, 187–195.

[3] Zhou Rui, Wang Qunjing, Li Guoli, Pang Cong and Fang Guanghui, *Optimal Design of Single-Phase Induction Motor Based on MAXWELL 2D Rmxprt, International conference on Electrical machines and Systems (ICEMS)*, 2010, 1367-1370.

[4] Meeker D.: *Finite Element Method Magnetics*, User's manual, Version 4.2 [online at <http://www.femm.info/wiki/HomePage>], 25 August 2013

[5] S. Williamson and M.J. Robinson, *Calculation of Cage Rotor Induction Motor Equivalent Circuit Parameters using Finite Elements, IEEE proceedings-B, Electric Power Applications*, Vol. 138, No.5, September 1991, 264-276.

[6] S. Salon, D. Burow, M. De Bortoli and C. Slavik, *Effects of Slot Closure and Magnetic Saturation on Induction Machine Behavior, IEEE Transactions on Magnetics*, Vol. 30, No. 5, 1994, 3697-3700.

[7] Gun Hee Jang and S. J. Park, *Characterization of a Single-Phase Induction Motor Due to the Effect of Slot Opening, IEEE Transactions on magnetics*, Vol. 40, No. 4, July 2004, 2065-2067.

[8] V. Fireteanu, T. Tudorache and O.A. Turcanu, *Optimal Design of Rotor Slot Geometry of Squirrel-Cage Type Induction Motors, International conference on Electric machines & drives conference (IEMDC)*, 2007, 537-542.

[9] Deliang Shan and Xinzhen Wu, *Rotor Resistance and Inductance Calculation of Single-Phase Induction Motors with Skin Effect Consideration, Electrical Machines and Systems (ICEMS)*, 2008, 79-82.

[10] Ashfaq Hussain, *Electrical Machines (2nd Edition)*, Dhanpat rai & co. (pvt.) Ltd. 2009, 549-552.

[11] Kwangsoo Kim, Seung-Bin Lim and Ju Lee, *Design of Rotor Slot of Single-Phase Induction Motor with Copper Die-Cast Rotor Cage for High Efficiency, International Telecommunications Energy Conference (INTELEC)*, 2009, 1-4.

[12] M.S. Alshamasin, *Optimization of the Performance of Single-Phase Capacitor-Run Induction Motor, American Journal of Applied Sciences*, 2009, 745-751.

- [13] M. Bose, A. Bhattacharjee and Sudha R., *Calculation of Induction Motor Model Parameters Using Finite Element Method, International Journal of Soft Computing and Engineering (IJSCE)*, Vol.2, No. 3, July 2012, 41-43.
- [14] Z.N. Gheidari and H. Lesani, *Optimal Design of Adjustable Air-Gap, Two-Speed, Capacitor-Run and Single-Phase Axial Flux Induction Motors, IEEE Transactions on energy conversion*, vol. 28, No. 3, September 2013, 543-552.
- [15] R. Cipin and Miroslav Patocka, *Skin Effect in Rotor Bars of Induction Motor in Form of Transfer Function, Industrial Electronics Society (IECON)*, 2013, 3149-3153.
- [16] Jalila Kaouther Kamoun et al., *An Induction Motor FEM-Based Comparative Study: Analysis of Two Topologies, International Conference and Exhibition on Ecological Vehicles and Renewable Energies (EVER)*, 2013, 1-5.
- [17] Y. Zhang and W. Hofmann, *Energy-Efficient Control of Induction Motors with High Torque Dynamics and Transient Skin Effect, Industrial Electronics Society (IECON)*, 2013, 2774-2779.
- [18] A.K. Sawhney, *A Course in Electrical Machine Design*, Dhanpat Rai & Co. (P) Ltd. India.